

This is an Open Access document downloaded from ORCA, Cardiff University's institutional repository: <https://orca.cardiff.ac.uk/id/eprint/128893/>

This is the author's version of a work that was submitted to / accepted for publication.

Citation for final published version:

Adams, Natalie E, Hughes, Laura E, Phillips, Holly N, Shaw, Alexander D, Murley, Alexander G, Nesbitt, David, Cope, Thomas E, Richard Bevan- Jones, W, Passamonti, Luca and Rowe, James B 2020. GABA-ergic dynamics in human frontotemporal networks confirmed by pharmacomagnetoencephalography. *Journal of Neuroscience* 40 (8), pp. 1640-1649. 10.1523/JNEUROSCI.1689-19.2019

Publishers page: <http://dx.doi.org/10.1523/JNEUROSCI.1689-19.2019>

Please note:

Changes made as a result of publishing processes such as copy-editing, formatting and page numbers may not be reflected in this version. For the definitive version of this publication, please refer to the published source. You are advised to consult the publisher's version if you wish to cite this paper.

This version is being made available in accordance with publisher policies. See <http://orca.cf.ac.uk/policies.html> for usage policies. Copyright and moral rights for publications made available in ORCA are retained by the copyright holders.



1 **Title:** GABA-ergic dynamics in human frontotemporal networks confirmed by pharmaco-  
2 magnetoencephalography.

3 **Abbreviated:** GABA networks by pharmaco-MEG.

4 **Authors:** Natalie E. Adams<sup>1</sup>, Laura E. Hughes<sup>1,2</sup>, Holly N. Phillips<sup>1</sup>, Alexander D. Shaw<sup>2</sup>, Alexander G.  
5 Murley<sup>1</sup>, David Nesbitt<sup>1</sup>, Thomas E. Cope, W. Richard Bevan-Jones, Luca Passamonti, James B.  
6 Rowe<sup>1,2</sup>

7 <sup>1</sup>Department of Clinical Neurosciences, Cambridge Biomedical Campus, University of Cambridge,  
8 Cambridge, CB2 0QQ, UK

9 <sup>2</sup>MRC Cognition and Brain Sciences Unit, 15 Chaucer Road, Cambridge, CB2 7EF, UK

10 <sup>3</sup>Cambridge Centre for Ageing and Neuroscience (Cam-CAN), University of Cambridge, UK

11 **Corresponding Author:** James B. Rowe, [james.rowe@mrc-cbu.cam.ac.uk](mailto:james.rowe@mrc-cbu.cam.ac.uk)

12 **Number of Pages:** 38

13 **Number of Figures:** 4

14 **Number of Tables:** 1

15 **Number of Words for Abstract:** 210

16 **Number of Words for Introduction:** 650

17 **Number of Words for Discussion:** 1489

18 **Conflict of Interest:** The authors declare no competing financial interests.

19 **Acknowledgements:** This work was funded by the Wellcome Trust (103838), the National Institute  
20 for Health Research Cambridge Biomedical Research Centre and the Medical Research Council

21 (MC\_U105597119; MC\_U\_00005/12; SUAG/004/91365), Cambridge Centre for Parkinson-plus and

22 the Holt Fellowship. A.D.S is supported by a Wellcome Trust Strategic Award (104943/Z/14/Z).

23 **Abstract**

24 To bridge the gap between preclinical cellular models of disease and *in vivo* imaging of human  
25 cognitive network dynamics, there is a pressing need for informative biophysical models. Here we  
26 assess dynamic causal models (DCM) of cortical network responses, as generative models of  
27 magnetoencephalographic observations during an auditory oddball roving paradigm in healthy  
28 adults. This paradigm induces robust perturbations that permeate frontotemporal networks,  
29 including an evoked ‘mismatch negativity’ response and transiently induced oscillations. Here, we  
30 probe GABAergic influences of the networks using double-blind placebo-controlled randomised-  
31 crossover administration of the GABA re-uptake inhibitor, tiagabine (oral, 10mg) in healthy older  
32 adults. We demonstrate the facility of conductance-based neural mass mean-field models,  
33 incorporating local synaptic connectivity, to investigate laminar-specific and GABAergic mechanisms  
34 of the auditory response. The neuronal model accurately recapitulated the observed  
35 magnetoencephalographic data. Using parametric empirical Bayes for optimal model inversion  
36 across both drug sessions, we identify the effect of tiagabine on GABAergic modulation of deep  
37 pyramidal and interneuronal cell populations. We found a transition of the main GABAergic drug  
38 effects from auditory cortex in standard trials to prefrontal cortex in deviant trials. The successful  
39 integration of pharmaco- magnetoencephalography with dynamic causal models of frontotemporal  
40 networks provides a potential platform on which to evaluate the effects of disease and  
41 pharmacological interventions.

42 **Significance Statement**

43 Understanding human brain function and developing new treatments require good models of brain  
44 function. We tested a detailed generative model of cortical microcircuits that accurately reproduced  
45 human magnetoencephalography, to quantify network dynamics and connectivity in frontotemporal  
46 cortex. This approach identified the effect of a test drug (GABA-reuptake inhibitor, tiagabine) on  
47 neuronal function (GABA-ergic dynamics), opening the way for psychopharmacological studies in  
48 health and disease with the mechanistic precision afforded by generative models of the brain.

49

## 50 **Introduction**

51 Biophysically informed models of cognition and cognitive disorders facilitate the effective translation  
52 of the mechanisms and treatments of disease. Recent progress towards detailed generative models  
53 that replicate neurophysiological correlates of cognition based on cellular and network dynamics,  
54 such as 'Dynamic Causal Models' (DCM), make predictions that approximate observations by  
55 functional magnetic resonance imaging or electro- and magneto-encephalography (MEG) (Moran et  
56 al., 2013). To be most useful, these models should incorporate laminar, cellular and synaptic  
57 functions (Bastos et al., 2012), and adhere to basic principles of cortical connectivity (Shipp, 2016),  
58 while also being sufficiently tractable and accurate to study cognition.

59 The DCM framework developed to meet these criteria, with applications in health and neurological  
60 disorders (Kiebel et al., 2008; Stephan et al., 2008; Boly et al., 2011; Marreiros et al., 2015). DCMs  
61 draw on empirical priors for synaptic time constants and conductances, together with a mean-field  
62 forward model. They are optimised to match the observed neurophysiological data. DCMs are  
63 supported by extensive data for face-validity (Stephan et al., 2008, 2015) and construct-validity (Razi  
64 et al., 2015), but they must also achieve predictive validity (Moran et al., 2014; Gilbert and Moran,  
65 2016; Shaw et al., 2018).

66 We tested the ability of DCMs to identify the effect of a pharmacological intervention. The DCMs  
67 were designed to model human frontotemporal cortical networks during an auditory oddball  
68 paradigm, with characteristic MEG responses to standard and deviant tones (<300ms). The  
69 differential response to these tones (the Mismatch Negativity, MMN) is abnormal in many  
70 neurological diseases (Boly et al., 2011; Naatanen et al., 2011; Hughes et al., 2013), reflecting a  
71 change in prediction errors in hierarchical frontotemporal networks (Garrido et al., 2009b; Phillips et  
72 al., 2015).

73 To examine laminar- and synaptic-dynamics in response to auditory stimuli we developed a new  
74 DCM with six cell populations, called "ext-DCM". In six connected regions (locations from Phillips et

75 al., 2015, 2016), we used a conductance-based mean-field cortical modelling scheme (cf. Moran et  
76 al., 2013; Marreiros et al., 2015). For auditory mismatch responses, both thalamocortical and  
77 cortico-cortical connections integrate feedforward sensory inputs and feedback expectations. The  
78 network architecture controls the flow and integration of information, via cell- and  
79 neurotransmitter-specific interactions. The ext-DCM introduces new cortico-thalamic burst-firing  
80 cells ('tp' in Figure 1a) that enable the model to generate beta activity from deep-layers (Roopun et  
81 al., 2008a, 2010; Bordas et al., 2015; Michalareas et al., 2016). The ext-DCM also separates the  
82 inhibitory interneuronal populations for superficial and deep pyramidal cells (e.g. Jiang *et al.*, 2015).  
83 These extensions improve the DCMs' functionality in terms of laminar dynamics. We tested the  
84 model's ability to accurately generate evoked magnetoencephalographic responses (i.e. event  
85 related fields, ERF), under placebo and drug conditions.

86 With the ext-DCM, we used the drug tiagabine to test how well the neurophysiological model could  
87 identify changes in the causes of observed neuronal dynamics. Tiagabine is a gamma-amino-butyric  
88 acid (GABA) re-uptake inhibitor. GABA is critical for the generation of physiological responses and  
89 rhythms in local and global processing (Whittington et al., 2000). This pharmacological specificity  
90 provides a more controlled acute test of DCMs than autoimmune (Symmonds et al., 2018) and  
91 genetic channelopathies (Gilbert et al., 2016).

92 Using parametric empirical Bayes to optimise the model across participants and drug conditions we  
93 examined how modelled GABAergic dynamics are altered by tiagabine. Based on the hypothesis that  
94 prediction and prediction error depend on short-term GABAergic plasticity (Castro-Alamancos and  
95 Connors, 1996; Garrido et al., 2009a; Mongillo et al., 2018; Spriggs et al., 2018), we predicted that  
96 upper and lower hierarchical frontotemporal processing would be differentially affected by tiagabine  
97 during standard and deviant tones.

98 In summary, the study's principal aims were i) to introduce and assess the ext-DCM for generating  
99 the event-related fields observed by MEG, ii) to identify receptor-specific changes that govern these  
100 dynamics, comparing tiagabine and placebo treatment conditions, and iii) to assess whether these

101 pharmacological effects are expressed dynamically across trial types and regions with laminar  
102 specificity.

103

104 **Materials and Methods**

105 *Experimental Design:*

106 We undertook a randomised placebo-controlled double-blind crossover study of the effects of  
107 tiagabine in 20 healthy adults (aged  $67.5 \pm 4.2$ , ten male). Participants had no neurological or  
108 psychiatric illness and were recruited from the MRC Cognition and Brain Sciences and Join Dementia  
109 Research volunteer panels. The study was approved by the Cambridge Research Ethics Committee  
110 and written informed consent was acquired, in keeping with the declaration of Helsinki.

111 Neurophysiological responses were measured in an auditory roving oddball paradigm (Garrido et al.,  
112 2008). Binaural sinusoidal tones were presented in phase via ear-pieces for 75 ms (with 7.5ms ramp  
113 up and down at start and end of the tone), at 500 ms intervals. The frequency of the tone increased  
114 or decreased in steps of 50 Hz (range 400 – 800 Hz). The change of frequency occurred after  
115 between 3 and 10 repetitions, with a truncated exponential distribution that approximated a stable  
116 expectancy of change over time. Auditory thresholds were assessed in quiet at 500, 1,000, and 1,500  
117 Hz. Tones were presented at 60dB above the average threshold for a standard population through  
118 the earpieces in the MEG.

119 Each participant attended two MEG sessions with a minimum two weeks interval. They received  
120 either 10 mg oral tiagabine or a placebo, in randomised order. Bloods were taken 105 minutes later,  
121 immediately prior to MEG data acquisition, to coincide with peak plasma levels and CNS penetration  
122 (Nutt et al., 2015).

123 *Data Acquisition and pre-processing:*

124 Magnetoencephalography (MEG) used a 306-channel Vectorview acquisition system (Elekta  
125 Neuromag, Helsinki) in a light Elekta Neuromag magnetically-shielded room. This consists of a pair of  
126 gradiometers and a magnetometer at each of 102 locations, sampled at 1000 Hz. Vertical and  
127 horizontal EOGs tracked eye movements and 5 head-position indicator coils tracked head position. A  
128 MEG-Compatible 70 channel EEG cap (EasyCap GmbH) using Ag/AgCl electrodes positioned



129 according to the 10-20 system was used concurrently. A 3D digitizer (Fastrak Polhemus Inc.,  
130 Colchester, VA) was used to record >100 scalp data points, nasion and bilateral pre-auricular  
131 fiducials. Subjects also underwent T1-weighted structural magnetic resonance imaging (MPRAGE  
132 sequence, TE = 2.9 msTR = 2000 ms, 1.1mm isotropic voxels) using a 3T Siemens PRISMA scanner.

133 MEG data pre-processing included head position alignment and movement compensation using 6  
134 headcoils, placed around the head on the EEG cap, and employed the temporal extension of Signal  
135 Space Separation with MaxFilter v2.2 (Elekta Neuromag). The auto-detection of bad channels was  
136 combined with manual input of any channels logged as bad during data acquisition. The Statistical  
137 Parametric Mapping toolbox (SPM12) (The Wellcome Trust Centre for Neuroimaging, UCL, UK) was  
138 used for further pre-processing and analysis, in conjunction with modified and custom MATLAB  
139 scripts (MATLAB 2017a, Mathworks, Natick, MA). Data were Butterworth filtered between 1 and 180  
140 Hz, epoched from -100 ms to 400 ms relative to the auditory stimuli and artefact rejected using EOG,  
141 EEG and MEG channel thresholding. Spectral analyses were performed using a multi-taper method.  
142 The deviant trial was taken as the 1<sup>st</sup> trial of a train, regardless of the frequency and the 6<sup>th</sup> trial of a  
143 train was modelled as 'standard'.

144 Source reconstruction used a forward model estimated using the single shell cortical mesh from  
145 each individual's T1-weighted MR structural scan. After co-registration using the fiducials and head  
146 points, local fields (LFs) for 6 sources of interest were source-reconstructed using SPM "COH"  
147 method, a combination of LORETA and minimum norm (Pascual-Marqui et al., 1994; Heers et al.,  
148 2016). Sources of interest were (with MNI coordinates in standard space following inverse  
149 normalisation): left auditory cortex (LAud; -42, -22, 7), left superior temporal gyrus (LSTG; -61 -32 8),  
150 left inferior frontal gyrus (LIFG; -46 20 8), right auditory cortex (RAud; 46, -14, 8), right superior  
151 temporal gyrus (RSTG; 59 -25 8) and right inferior frontal gyrus (RIFG; 46 20 8). To create images of  
152 induced power, SPM-LORETA was used for source localization of a 5 mm<sup>3</sup> regular grid at the MMN  
153 (150 – 250 ms) time window (100ms in width, regularization=0.05).

154 Correlation coefficients for comparing the actual and predicted ERFs were calculated using the  
155 `corrcoef` function (Pearson correlation) in MATLAB 2017a for each individual, condition and node.

156 Time-frequency analysis was performed in SPM12 using a multi-taper method with 100 ms windows  
157 overlapped by 5 ms and a bandwidth of 3. Frequency bands were split into alpha (8 – 13 Hz), beta  
158 (14 – 29 Hz), low gamma (30 – 48 Hz) and high gamma (52 – 80 Hz).

### 159 *Neuronal Modelling: an extended canonical microcircuit model*

160 We used conductance-based canonical mean field (CMM) models for evoked responses (Kiebel et al.,  
161 2008) utilising canonical microcircuit models (SPM12, DCM10). This approach to  
162 neurophysiologically informed modelling using DCM goes beyond descriptive biomarkers by  
163 providing a mechanistic link to realistic microscopic processes. A common approach in DCM is to  
164 invert the neuronal and spatial forward model as a single generative model, to solve the source  
165 reconstruction and biophysical modelling problems jointly by fitting the DCM to sensor data.  
166 However, we modelled source specific responses to suppress conditional dependencies between the  
167 neuronal parameters and the parameters of a spatial forward model. This affords more efficient  
168 estimators of neuronal parameters, providing the source reconstruction is sufficiently precise given  
169 the spatial topography of the network of interest. This has the advantage of compatibility with  
170 multiple studies of this task (Muthukumaraswamy et al., 2015; Gilbert and Moran, 2016; Shaw et al.,  
171 2017, 2018), including MEG and electrocorticography studies; the chosen network was based on the  
172 published bilateral A1, STG, IFG networks associated with the generation of the MMN response.  
173 Since this spatial element of the inverse problem was constrained, it is computationally more  
174 appropriate to source localise using SPM with prior expected sources. The subsequent DCM was  
175 then run on these virtual electrodes.

176 Our DCM included a conductance-based neural-mass model at each of the six anatomical locations,  
177 as shown in Figure 1. We compared the default 4-cell conductance canonical-microcircuit model  
178 with the ext-DCM, comprising 6 cell modules: a superficial pyramidal module (sp), a deep cortico-

179 cortical pyramidal module (dp), a thalamic-projection pyramidal module (tp), a granular stellate  
180 module (ss) and separate supragranular and infragranular interneuron populations (si & di).  
181 Excitatory autapses existed for all excitatory cell modules and all modules were also governed by an  
182 inhibitory self-gain function that provided tonic inhibition to each module. The ext-DCM was  
183 compared to the standard 4-cell model that is standard in SPM and is described in detail in Kiebel et  
184 al. (2008). In summary, the 4-cell DCM lacks thalamocortical connectivity and has a unitary inhibitory  
185 population interacting with all pyramidal and stellate cell populations.

186 The intrinsic connectivities are shown in Fig. 1a: note the excitatory conductances based on AMPA  
187 and NMDA and inhibitory GABA-A and GABA-B conductances. The model is an extension of the SPM  
188 conductance-based CMM model (SPM12, 2013): inclusion of separate supra- and infra-granular  
189 interneuron populations creates a more biophysically realistic model that allows a greater flexibility  
190 of independence of deep and superficial activity than in previous work (Bhatt et al., 2016; Shaw et  
191 al., 2018; Spriggs et al., 2018). Additionally, the new 'tp' population expressed a hyperpolarization-  
192 activated cation current (H-current) and a non-inactivating potassium current (M-current) to provide  
193 surrogate intrinsic dynamics involved in the characteristic intrinsic bursting behaviour of these cells.  
194 These two currents were fixed together with the reversal potential and the slope on the sigmoid  
195 convolution of in-activation for the H-current (details of which parameters had a permitted variance  
196 is given in Table 1). This, coupled with the cell capacitances, differentiates the intrinsic activation of  
197 the 'tp' population from the 'dp' population. The populations also differed in their extrinsic  
198 connectivities, with 'dp' populations forming cortico-cortical connections and 'tp' populations  
199 allowing for cortico-thalamocortical connections. The thalamus was modelled implicitly, by an 80 ms  
200 delay in connectivity with permitted variance.

201 Extrinsic connectivity between the six nodes is shown in Fig. 1b, with the detailed extrinsic  
202 population connections shown in Fig. 1c. In keeping with the established principle of differential  
203 cortical laminar projections of feed-forwards vs feedback connectivity (Bastos et al., 2012), backward  
204 connections are facilitated by the 'dp' cells terminating on 'sp' and 'si' cells, whilst forward

205 connections run from 'sp' cells to 'ss' cells. Cortico-thalamo-cortical connections originate from 'tp'  
206 cells and terminate following a thalamic delay at layer 4 'ss' cells. The presence or absence of  
207 connections between nodes was based on the fully connected models from Phillips et al., (2015) and  
208 Shaw et al., (2019), which in turn were derived from Garrido et al., (2008). This was used for the  
209 basis of an iterative process to find the most likely reduced model (described below).

210 A Gaussian kernel (peak 60 ms, half-width 8 ms) represented auditory input to layer 4 stellates in  
211 bilateral auditory and inferior frontal cortex.

### 212 *Bayesian Modelling and Statistical Analysis:*

213 We used Bayesian model inversion (estimation) and Bayesian model comparison (selection) to  
214 identify the best explanation for subject-specific data, in terms of neuronal and biophysical  
215 parameters. Parametric Empirical Bayes (PEB) was used for group inferences and to examine drug  
216 effects, as described in Zeidman et al., (2019). By inverting a 'full' DCM per subject at the first level,  
217 PEB avoids the problem of different first level DCMs falling into different local optima, and allows  
218 subsequent comparison between conditions. At the second level, the parameters of interest were  
219 included in the PEB, namely the GABAA synaptic connections. This restricted set of second level  
220 parameters was oriented to our GABA-ergic hypothesis, and to improve stability of neural system  
221 identifiability.

222 The DCM was run for each subject. Data were filtered between 0–48 Hz and a Tukey window was  
223 applied that did not attenuate signals 50 ms before or 350 ms after stimuli. Inversion of the full  
224 model was run separately for the standard and deviant trials and the parameter distributions passed  
225 to second level Parametric Empirical Bayesian with contrasts for both trial types and drug conditions.  
226 All intrinsic and extrinsic AMPA, NMDA and GABA-A conductance scalings could vary independently  
227 in a manner that assumed symmetry between the two hemispheres. The prior means and permitted  
228 variances are summarised in Table 1.

229 Variational Bayesian statistics using the Laplace approximation determined the probable parameter  
230 space given the neuronal model and the data (Friston et al., 2007). The full model parameter space  
231 was reduced by iteratively searching for dependencies in this parameter space and systematically  
232 removing parameters not contributing to the free energy of the system (Henson et al., 2011). The  
233 optimised reduced model comprises all those parameters and connections found to contribute  
234 significantly to the system temporal dynamics. The comparison of full and reduced models is  
235 conceptually analogous to F-tests in classical statistics, but inferences are Bayesian. A second-level  
236 PEB was run, optimizing GABAA-ergic synaptic parameters (representing inhibitory gain). This second  
237 level PEB identifies parameter that are estimated to differ significantly between task conditions, or  
238 differ between drug-sessions, or for which there is a drug-by-condition interaction. The parameter  
239 distributions from this reduced model were used to create a Bayesian model average of parameters  
240 that differ significantly across the contrasts of trial types and drug conditions. The implementation of  
241 PEB for model optimisation and contrast estimation is summarised in Fig. 1e.

242 For other data types, Bayesian t-tests reported in the main text used JASP (JASP Team 2019, version  
243 0.10.2). Frequentist statistical methods reported in the main text used MATLAB (2017a, Mathworks,  
244 Natick, MA).

245 *Code Accessibility:* The custom neuronal model used to generate these results is available  
246 at <https://gitlab.com/tallie/edcm> and works in conjunction with SPM12.

247

248 **Results**

249 *Event related fields and induced spectral power*

250 Event related responses to standard and deviant trials were in line with previous findings (Hughes  
251 and Rowe, 2013; Phillips et al., 2015, 2016) (Fig. 2a, first and second rows) and show the expected  
252 M100, the primary response after the onset of a tone (80-120 ms), a difference signal (MMN)  
253 between the standard and deviant trials (150-250 ms) and an M300 visible in frontal nodes (250-380  
254 ms). The M100 was significantly reduced by tiagabine on standard and deviant trials, in left temporal  
255 nodes (A1, and STG  $p < 0.05$ , paired t-test), whereas the later response leading into the M300 was  
256 significantly reduced only on deviant trials in L/R IFG ( $p < 0.05$ , Bonferroni corrected for 6 regions).

257 The difference waveform (i.e. the deviant – the standard) reveals a typical biphasic MMN between  
258 150-250ms, observed in primary auditory cortex and STG (Fig. 2a, third row). Tiagabine significantly  
259 reduced the second peak of the MMN ( $p < 0.05$ ) with bilateral IFG nodes and RSTG showing  
260 reductions in the first peak of the mismatch response on tiagabine ( $p < 0.05$ ). As with the deviant  
261 response, LIFG showed a significant reduction of the later MMN peak and the M300 on tiagabine  
262 ( $p < 0.05$ ).

263 The temporal profile of spectral power differences (see Methods for time-frequency analysis)  
264 matched that of the ERFs, including spectral counterparts to M100, MMN, continuing through the  
265 M300 window (Fig. 2b&c). During the M100, alpha-power (8-12 Hz) decreases on tiagabine were  
266 localized to temporal cortex and beta (14-29 Hz) decreases more prominently to posterior temporal  
267 cortex. During the MMN, increases in low and high gamma (30-48 Hz and 52-80 Hz respectively)  
268 were observed broadly across right frontal cortex, including IFG. Low gamma also showed increases  
269 in right temporal cortex.

270 Such changes in the observed spatiotemporal physiology on tiagabine will be dependent on changes  
271 in local and global network connectivity. The extended conductance-based dynamic causal model  
272 was therefore used to infer the causes of the observed physiological changes.

273 *The Dynamical Causal Model:*

274 The residuals (difference between the actual and generated ERFs) were greater (worse) for the 4-cell  
275 DCM than for the ext-DCM (Bayesian paired sample t-test:  $BF=8.5 \times 10^{28}$ ) as shown in Fig. 3a. Bayesian  
276 model comparison of the 4-cell *versus* ext-DCM confirmed that the ext-DCM performed better (ie.  
277 was a more likely generator of the observed MEG) than the 4-cell DCM ( $BF = 40.6$ , Figure 3b). Note  
278 that the model-evidences are corrected for differences in model complexity. Further analyses use  
279 the ext-DCM only.

280 Fig. 3c demonstrates the evoked-response generated by the conductance-based dynamic causal  
281 model at each node, for both drug conditions, using the optimal ext-DCM model as determined by  
282 Parametric Empirical Bayes (see methods). Fig. 3d shows the correlation between generated and  
283 observed data, for both standards' and deviants' responses, for both drug conditions at each node.  
284 Boxplots indicate the spread of single-subject correlations across the group (open circles are  
285 outliers), and black closed circles indicate the correlation of the mean response across all subjects  
286 for each condition and node. Note how the periods of difference between the placebo and drug  
287 conditions (black lines in Fig. 3c) are accurately generated (cf. 'predicted') by the model, with a high  
288 match to the observed data in Fig. 2a.

289 The modelled responses are explained in terms of the parameters of the optimised model. Using  
290 parametric empirical Bayes, condition effects on model parameters (connection and synaptic  
291 parameters) were compared across the standard and deviant conditions, as well as across the  
292 placebo and tiagabine conditions. Figure 4 shows the effect of tiagabine on the intrinsic GABAergic  
293 connectivity, assuming symmetry (three bilateral averaged nodes are shown). We confirmed that  
294 tiagabine significantly increases tonic GABAergic inhibition (posterior probability given for each  
295 parameter in Fig. 4a). This was seen primarily in the deep layer pyramidal and interneuron  
296 populations in primary auditory cortex and STG (Fig. 4a). An interaction between drug and condition  
297 was found for the deep interneurons of Auditory cortex (posterior  $p \approx 1.0$ ).

298 Fig. 4b compares GABA-A conductance scaling on deep interneurons between placebo and tiagabine  
299 conditions, plotted for each individual. There was very strong evidence for differences between the  
300 two drug conditions in primary auditory areas for the standard condition (BF=782356), and in IFG  
301 and STG for the deviant condition (BF=3.58x10<sup>7</sup> & BF=166 respectively). This difference between  
302 primary auditory cortex and association cortex in STG/IFG, is in keeping with the functional  
303 differentiation of upper versus lower levels in a hierarchical neural network with backwards  
304 prediction and forward prediction error. Conversely, there was evidence of no difference between  
305 the two drug conditions for the standard condition in IFG (BF=0.274) and for the deviant condition in  
306 Aud (BF=0.241).

307 The correlation between tonic and phasic inhibition was explored for each region and condition. In  
308 the frontal cortex, a strong negative relationship was found between the tonic inhibition of deep  
309 inhibitory cells and their phasic inhibition onto cortico-thalamic cells (Fig. 4c Bayesian correlation  
310 pairs, BF=398.43).

311



## 312 Discussion

313 The principal insights from this study are that an extended conductance-based canonical mean-field  
314 method of dynamic causal modelling (a) succeeds in identifying the modulation of GABAergic  
315 dynamics by the GABA-reuptake inhibitor tiagabine, and (b) is tractable and an accurate generator of  
316 event-related fields that match those observed by magnetoencephalography, improving on an  
317 earlier 4-cell model. Moreover, the ext-DCM suggests the effect of drug to be both laminar-specific  
318 and dynamically modulated in different regions according to task condition. This opens the way for  
319 psychopharmacological studies in health and disease with the mechanistic precision afforded by  
320 using ext-DCMs as generative models.

321 We demonstrate that the intrinsic connectivity within hierarchical brain networks changes between  
322 conditions in the mismatch task. The approach is of generalised relevance to hierarchical network  
323 models of cognition such as speech (Cope et al., 2018), semantic (Adams et al., 2019) and visual  
324 perception (Muthukumaraswamy *et al.*, 2013). Moreover, the laminar and pharmacological  
325 specificity provided by the ext-DCM has the potential to quantify neuropathology in dementia,  
326 developmental and psychiatric disorders (Duyckaerts et al., 1986; Kinoshita et al., 1996; Ferrer,  
327 1999; Ji et al., 2018; Shaw et al., 2018).

328 *Understanding the MMN in terms of short-term plasticity.*

329 Tiagabine modulated the GABA-ergic dynamics across the trial types, implicating both local tonic- and  
330 phasic effects. Repetitive activation with the same stimulus attenuated the ERF (reduction in N1/N2  
331 by 6<sup>th</sup> repetition, Fig. 2). The model indicated higher tonic inhibition in the deep layers. We interpret  
332 this as local short-term plastic changes in deep-layer inhibition (Knott et al., 2002; Hensch, 2005;  
333 Jääskeläinen et al., 2007), regulating salient information (Mongillo et al., 2018).

334 The model suggested that tiagabine-induced increases of extracellular GABA leads to greater tonic  
335 inhibition, consistent with overspill of GABA onto extra-synaptic receptors (Semyanov et al., 2004).

336 The effect was modulated differently in primary and associative processing areas: for tonic inhibition

337 of deep interneurons the drug's efficacy was highest in prefrontal cortex for deviant trials and in  
338 auditory cortex for standard trials. In other words, GABAergic effects are modulated differentially in  
339 upper and lower areas of the hierarchy dependent on the coding context. We speculate that this  
340 reflects differential emphasis on beliefs (& feedback predictions) *versus* feedforward sensory  
341 prediction errors in prefrontal versus primary auditory cortex; and that lower tonic inhibition at the  
342 presentation of a deviant tone relates to homeostatic competition between phasic and tonic  
343 inhibition (Wu et al., 2013). Increased phasic activation of deep-layer projections is necessary for  
344 feedback of top-down information on context, which in turn increases phasic (and decreased tonic)  
345 activation of deep interneurons. Decreasing tonic inhibition likely increases the interneuron  
346 population activation (Semyanov et al., 2004), leading to increased phasic inhibition onto deep  
347 pyramidal cells. This relationship was confirmed (Fig. 4c) between tonic inhibition of deep IFG  
348 interneurons and phasic inhibition of deep IFG thalamic-projection neurons. Figure 4b shows that  
349 whereas a drop in deep interneuron tonic inhibition was observed on deviant trials (*vs* standard),  
350 tiagabine abolished the effect. It is to be expected that increases in exogenous GABA would increase  
351 tonic GABAergic currents.

352 *GABA-ergic modulation of evoked and induced responses.*

353 Tiagabine affects oscillatory dynamics, which may influence behaviour (Coenen et al., 1995;  
354 Magazzini et al., 2016; Port et al., 2017; Wyss et al., 2017). It remains a challenge to relate systemic  
355 drug effects with local frequency-spectral phenomena. It has been proposed that beta-band activity  
356 is associated with infragranular cortical projection neurons with intrinsically bursting profiles (Groh  
357 et al., 2010; Roopun et al., 2010; Kim et al., 2015). We found that Tiagabine reduced the induced  
358 beta-band activity in temporal areas. The model suggests that tonic inhibition is increased on  
359 intrinsically bursting thalamic projection neurons in STG, which could increase rebound bursting via  
360 intrinsic M- and H-currents (Roopun *et al.*, 2008; Roopun *et al.*, 2008b).

361 Conversely, it has been shown that gamma-band activity is dependent on the GABA-A receptor  
362 activation and the phasic interplay of interneuron-pyramidal cell networks, particularly in the

363 superficial layers (Buffalo et al., 2011; Whittington et al., 2011). In the mismatch temporal window  
364 (Fig. 2b) peak gamma increased occurring at the start of the mismatch period. This is consistent with  
365 thalamic input (Di and Barth, 1992, 1993; Sukov and Barth, 2001) governing the envelope of gamma  
366 activity in the superficial layers (Metherate and Cruikshank, 1999).

367 Overall, the observed dynamics and the model posterior parameters are consistent with knowledge  
368 of network activation within the context of beta- and gamma- rhythm generation in cortex.

### 369 *Generative models of drug effects on cognitive physiology.*

370 Tiagabine's effect was largely confined to deep layers. As we modelled evoked activity it is difficult to  
371 speculate on how this influences gamma activity across the network, however a reduction in deep-  
372 layer influence may increase local cortical processing associated with gamma-band activity in the  
373 superficial layers. As GABA levels are typically lower in older *versus* younger adults, tiagabine may  
374 act 'restoratively'. This is corroborated with lower frequency responses that are dependent on GABA  
375 (Mathias et al., 2001). Finally, we speculate that the reduced M100 on tiagabine results from the  
376 widespread increased tonic inhibition represented in the model (Fig. 4), reducing local population  
377 activity.

### 378 *Study limitations.*

379 Our study was motivated by the need for mechanistic studies of human cortical function, underlying  
380 cognition, disease and therapeutics. Despite support for our three principal hypotheses, and  
381 background validation studies (Moran et al., 2014), evidence from one study may not generalise to  
382 other tasks and populations. There are study-specific considerations that limit our inferences, in  
383 relation to our participants, our model, and drug of choice. For example, our participants were  
384 healthy, and therefore have normal age related variance in GABA (Gao et al., 2013; Eavri et al.,  
385 2018). They were older than those studied by Nutt et al (2015), and age-effects could interact with  
386 the effects of tiagabine (Nutt et al., 2015). Our study was not designed to examine the effect of age

387 or ageing, but to focus on the normal brain in mid- and later-life. Further work would be required to  
388 examine the effects of ageing on the ext-DCM.

389 Our model provides a simplified substrate for the neurophysiological processes. It is more detailed  
390 than previous canonical microcircuit convolution models (Moran et al., 2013), in an effort to improve  
391 the modelling of specific dynamics from distinct cell populations, their differing connectivities,  
392 synaptic time constants and voltage-gated conductances. The extended model can produce a  
393 spectrum of fast and slow responses, with fast responses involved in local processing dominated by  
394 superficial layers and slower responses associated with feedback of information dominated by deep  
395 layers (Roopun et al., 2006; Kramer et al., 2008; Whittington et al., 2011). It can incorporate delayed  
396 activity associated with local, cortico-cortical and cortico-thalamo-cortical connections. Currently,  
397 this system is a simplified network acting as a neural mass, and can represent relevant cortical  
398 interactions involved in ERF generation in the context of this task and study. It does this by allowing  
399 forward and backward modulation of activity between deep and superficial layers, where synaptic  
400 time constants corroborate with standard GABA, NMDA and AMPA receptor decays. The six  
401 specified nodes are commonly cited in the literature in the context of this task (Garrido et al., 2009b;  
402 Phillips et al., 2015). Although they are not a complete representation of possible network  
403 configurations, they have been shown to capture critical aspects of cortical function: here the  
404 network has been supplemented with modelled exogenous and endogenous inputs via thalamus.

405 We emphasise Bayesian statistical analyses over classical frequentist methods. Where parameter  
406 estimates derived from earlier DCMs are used for frequentist statistical tests, they have excellent  
407 reliability across sessions, and similar power to fMRI and EEG studies (Rowe et al., 2010; Goulden et  
408 al., 2012; Bernal-Casas et al., 2013). Frequentist approaches are familiar to many readers, and have  
409 been the norm for comparison of ERFs, and we therefore include them selectively. Such a  
410 frequentist approach is surpassed by the direct inferences on posterior probability inherent in DCMs  
411 Bayesian inference, including PEB.

412 Tiagabine is a relatively specific blocker of GAT-1 at the concentrations used, but does not  
413 distinguish between the mechanisms activated by GABA (Bowery et al., 1987; Mody and Pearce,  
414 2004; Lee and Maguire, 2014). The timing of the magnetoencephalography coincided with expected  
415 peak plasma levels, but levels may vary between individuals and future studies could include levels  
416 as a covariate of interest, or model time-varying responses in relation to drug levels  
417 (Muthukumaraswamy et al., 2013b).

418 In conclusion, we have used a conductance-based model of cortical neuronal dynamics to study  
419 GABA-ergic interactions and probe laminar-specific physiological responses to tiagabine. The model  
420 accurately generated physiological data that matched the MEG responses and confirmed the effect  
421 of tiagabine on tonic GABA-A inhibitory gain within frontal and temporal cortical circuits. Our data  
422 provide support for mechanistic studies of neurological disorders, including but not limited to  
423 GABAergic impairments (Murley and Rowe, 2018). They also point to new approaches for  
424 experimental medicine studies in humans that aim for the laminar, cellular or synaptic precision  
425 made possible in new generations of dynamic causal models.

426

427

428 **Acknowledgements**

429 This work was funded by the Wellcome Trust (103838), the National Institute for Health Research  
430 Cambridge Biomedical Research Centre and the Medical Research Council (MC\_U105597119 &  
431 MC\_U\_00005/12), Cambridge Centre for Parkinson-plus and Holt Fellowship. We thank the PSP  
432 Association & FTD Support Group for raising awareness of the study.

433

434

435 **References**

- 436 Adams NE, Teige C, Mollo G, Karapanagiotidis T, Cornelissen PL, Smallwood J, Traub RD, Jefferies E,  
437 Whittington MA (2019) Theta/delta coupling across cortical laminae contributes to semantic  
438 cognition. *J Neurophysiol*:jn.00686.2018 Available at:  
439 <https://www.physiology.org/doi/10.1152/jn.00686.2018> [Accessed January 31, 2019].
- 440 Bastos AM, Usrey WM, Adams RA, Mangun GR, Fries P, Friston KJ (2012) Canonical Microcircuits for  
441 Predictive Coding. *Neuron* 76:695–711 Available at:  
442 <https://www.sciencedirect.com/science/article/pii/S0896627312009592> [Accessed January 15,  
443 2019].
- 444 Bernal-Casas D, Balaguer-Ballester E, Gerchen MF, Iglesias S, Walter H, Heinz A, Meyer-Lindenberg A,  
445 Stephan KE, Kirsch P (2013) Multi-site reproducibility of prefrontal–hippocampal connectivity  
446 estimates by stochastic DCM. *Neuroimage* 82:555–563 Available at:  
447 <https://www.sciencedirect.com/science/article/pii/S1053811913006307> [Accessed March 1,  
448 2019].
- 449 Bhatt MB, Bowen S, Rossiter HE, Dupont-Hadwen J, Moran RJ, Friston KJ, Ward NS (2016)  
450 Computational modelling of movement-related beta-oscillatory dynamics in human motor  
451 cortex. *Neuroimage* 133:224–232 Available at:  
452 <https://www.sciencedirect.com/science/article/pii/S1053811916001981#f0005> [Accessed  
453 January 15, 2019].
- 454 Boly M, Garrido MI, Gosseries O, Bruno M-A, Boveroux P, Schnakers C, Massimini M, Litvak V,  
455 Laureys S, Friston K (2011) Preserved Feedforward But Impaired Top-Down Processes in the  
456 Vegetative State. *Science (80- )* 332:858–862 Available at:  
457 <http://www.ncbi.nlm.nih.gov/pubmed/21566197> [Accessed February 26, 2019].
- 458 Bordas C, Kovacs A, Pal B (2015) The M-current contributes to high threshold membrane potential  
459 oscillations in a cell type-specific way in the pedunculo pontine nucleus of mice. *Front Cell*

460 Neurosci 9:121 Available at:  
461 <http://journal.frontiersin.org/article/10.3389/fncel.2015.00121/abstract> [Accessed March 1,  
462 2019].

463 Bowery NG, Hudson AL, Price GW (1987) GABAA and GABAB receptor site distribution in the rat  
464 central nervous system. *Neuroscience* 20:365–383 Available at:  
465 <https://www.sciencedirect.com/science/article/pii/0306452287900984> [Accessed September  
466 11, 2018].

467 Buffalo EA, Fries P, Landman R, Buschman TJ, Desimone R (2011) Laminar differences in gamma and  
468 alpha coherence in the ventral stream. *Proc Natl Acad Sci U S A* 108:11262–11267.

469 Castro-Alamancos MA, Connors BW (1996) Cellular mechanisms of the augmenting response: short-  
470 term plasticity in a thalamocortical pathway. *J Neurosci* 16:7742–7756 Available at:  
471 <http://www.ncbi.nlm.nih.gov/pubmed/8922430> [Accessed June 19, 2018].

472 Coenen AML, Blezer EHM, van Luijtelaar ELJM (1995) Effects of the GABA-uptake inhibitor tiagabine  
473 on electroencephalogram, spike-wave discharges and behaviour of rats. *Epilepsy Res* 21:89–94  
474 Available at: <https://www.sciencedirect.com/science/article/pii/0920121195000153> [Accessed  
475 February 26, 2019].

476 Di S, Barth DS (1992) The functional anatomy of middle-latency auditory evoked potentials:  
477 thalamocortical connections. *J Neurophysiol* 68:425–431 Available at:  
478 <http://www.ncbi.nlm.nih.gov/pubmed/1382119> [Accessed September 5, 2018].

479 Di S, Barth DS (1993) Binaural vs. monaural auditory evoked potentials in rat neocortex. *Brain Res*  
480 630:303–314 Available at:  
481 <https://www.sciencedirect.com/science/article/pii/0006899393906701> [Accessed September 5,  
482 2018].

483 Duyckaerts C, Hauw J-J, Bastenaire F, Piette F, Poulain C, Rainsard V, Javoy-Agid F, Berthaux P (1986)



484 Laminar distribution of neocortical senile plaques in senile dementia of the alzheimer type.  
485 Acta Neuropathol 70:249–256 Available at: <http://link.springer.com/10.1007/BF00686079>  
486 [Accessed January 15, 2019].

487 Eavri R, Shepherd J, Welsh CA, Flanders GH, Bear M, Nedivi E (2018) Interneuron simplification and  
488 loss of structural plasticity as markers of aging-related functional decline. J Neurosci:0808–  
489 0818 Available at: <http://www.ncbi.nlm.nih.gov/pubmed/30108129> [Accessed August 22,  
490 2018].

491 Ferrer I (1999) Neurons and their dendrites in frontotemporal dementia. Dement Geriatr Cogn  
492 Disord 10 Suppl 1:55–60 Available at: <http://www.ncbi.nlm.nih.gov/pubmed/10436342>  
493 [Accessed August 22, 2018].

494 Friston K, Mattout J, Trujillo-Barreto N, Ashburner J, Penny W (2007) Variational free energy and the  
495 Laplace approximation. Neuroimage 34:220–234 Available at:  
496 <https://www.sciencedirect.com/science/article/pii/S1053811906008822> [Accessed May 1,  
497 2018].

498 Gao F, Edden RAE, Li M, Puts NAJ, Wang G, Liu C, Zhao B, Wang H, Bai X, Zhao C, Wang X, Barker PB  
499 (2013) Edited magnetic resonance spectroscopy detects an age-related decline in brain GABA  
500 levels. Neuroimage 78:75–82 Available at:  
501 <https://www.sciencedirect.com/science/article/pii/S105381191300339X> [Accessed September  
502 4, 2018].

503 Garrido MI, Friston KJ, Kiebel SJ, Stephan KE, Baldeweg T, Kilner JM (2008) The functional anatomy of  
504 the MMN: a DCM study of the roving paradigm. Neuroimage 42:936–944 Available at:  
505 <https://linkinghub.elsevier.com/retrieve/pii/S1053811908006484> [Accessed January 8, 2019].

506 Garrido MI, Kilner JM, Kiebel SJ, Stephan KE, Baldeweg T, Friston KJ (2009a) Repetition suppression  
507 and plasticity in the human brain. Neuroimage 48:269–279 Available at:  
508 <https://www.sciencedirect.com/science/article/pii/S1053811909006661> [Accessed January 8,

509 2019].

510 Garrido MI, Kilner JM, Stephan KE, Friston KJ (2009b) The mismatch negativity: a review of  
511 underlying mechanisms. *Clin Neurophysiol* 120:453–463 Available at:  
512 <http://www.ncbi.nlm.nih.gov/pubmed/19181570> [Accessed May 1, 2018].

513 Gilbert JR, Moran RJ (2016) Inputs to prefrontal cortex support visual recognition in the aging brain.  
514 *Sci Rep* 6:31943 Available at: <http://www.nature.com/articles/srep31943> [Accessed January  
515 14, 2019].

516 Gilbert JR, Symmonds M, Hanna MG, Dolan RJ, Friston KJ, Moran RJ (2016) Profiling neuronal ion  
517 channelopathies with non-invasive brain imaging and dynamic causal models: Case studies of  
518 single gene mutations. *Neuroimage* 124:43–53 Available at:  
519 <https://www.sciencedirect.com/science/article/pii/S1053811915007788> [Accessed July 8,  
520 2019].

521 Goulden N, Elliott R, Suckling J, Williams SR, Deakin JFW, McKie S (2012) Sample Size Estimation for  
522 Comparing Parameters Using Dynamic Causal Modeling. *Brain Connect* 2:80–90 Available at:  
523 <http://www.liebertpub.com/doi/10.1089/brain.2011.0057> [Accessed March 1, 2019].

524 Groh A, Meyer HS, Schmidt EF, Heintz N, Sakmann B, Krieger P (2010) Cell-Type Specific Properties of  
525 Pyramidal Neurons in Neocortex Underlying a Layout that Is Modifiable Depending on the  
526 Cortical Area. *Cereb Cortex* 20:826–836 Available at:  
527 <http://www.ncbi.nlm.nih.gov/pubmed/19643810> [Accessed June 19, 2018].

528 Heers M, Chowdhury RA, Hedrich T, Dubeau F, Hall JA, Lina J-M, Grova C, Kobayashi E (2016)  
529 Localization Accuracy of Distributed Inverse Solutions for Electric and Magnetic Source Imaging  
530 of Interictal Epileptic Discharges in Patients with Focal Epilepsy. *Brain Topogr* 29:162–181  
531 Available at: <http://link.springer.com/10.1007/s10548-014-0423-1> [Accessed December 18,  
532 2018].

533 Hensch TK (2005) Critical period plasticity in local cortical circuits. *Nat Rev Neurosci* 6:877–888  
534 Available at: <http://www.nature.com/articles/nrn1787> [Accessed August 22, 2018].

535 Henson RN, Wakeman DG, Litvak V, Friston KJ (2011) A Parametric Empirical Bayesian Framework for  
536 the EEG/MEG Inverse Problem: Generative Models for Multi-Subject and Multi-Modal  
537 Integration. *Front Hum Neurosci* 5:76 Available at:  
538 <http://journal.frontiersin.org/article/10.3389/fnhum.2011.00076/abstract> [Accessed May 1,  
539 2018].

540 Hughes LE, Ghosh BCP, Rowe JB (2013) Reorganisation of brain networks in frontotemporal  
541 dementia and progressive supranuclear palsy. *NeuroImage Clin* 2:459–468 Available at:  
542 <https://www.sciencedirect.com/science/article/pii/S2213158213000302> [Accessed October 24,  
543 2018].

544 Hughes LE, Rowe JB (2013) The Impact of Neurodegeneration on Network Connectivity: A Study of  
545 Change Detection in Frontotemporal Dementia. *J Cogn Neurosci* 25:802–813 Available at:  
546 [http://www.mitpressjournals.org/doi/10.1162/jocn\\_a\\_00356](http://www.mitpressjournals.org/doi/10.1162/jocn_a_00356) [Accessed January 15, 2019].

547 Jääskeläinen IP, Ahveninen J, Belliveau JW, Raij T, Sams M (2007) Short-term plasticity in auditory  
548 cognition. *Trends Neurosci* 30:653–661 Available at:  
549 <https://www.sciencedirect.com/science/article/pii/S0166223607002585> [Accessed June 26,  
550 2018].

551 Ji E, Samuel S, Leboyer M, Guevara M, Guevara P, Poupon C, Grigis A, Houenou J (2018) T145.  
552 ALTERATIONS IN SUPERFICIAL WHITE MATTER IN THE FRONTAL CORTEX IN SCHIZOPHRENIA: A  
553 DWI STUDY USING A NOVEL ATLAS. *Schizophr Bull* 44:S172–S172 Available at:  
554 [https://academic.oup.com/schizophreniabulletin/article/44/suppl\\_1/S172/4957486](https://academic.oup.com/schizophreniabulletin/article/44/suppl_1/S172/4957486) [Accessed  
555 January 15, 2019].

556 Jiang X, Shen S, Cadwell CR, Berens P, Sinz F, Ecker AS, Patel S, Tolias AS (2015) Principles of  
557 connectivity among morphologically defined cell types in adult neocortex. *Science* (80- )

558 350:aac9462–aac9462 Available at: <http://www.ncbi.nlm.nih.gov/pubmed/26612957>  
559 [Accessed March 1, 2019].

560 Kiebel SJ, Garrido MI, Moran RJ, Friston KJ (2008) Dynamic causal modelling for EEG and MEG. *Cogn*  
561 *Neurodyn* 2:121–136 Available at: <http://link.springer.com/10.1007/s11571-008-9038-0>  
562 [Accessed January 14, 2019].

563 Kim EJ, Juavinett AL, Kyubwa EM, Jacobs MW, Callaway EM (2015) Three Types of Cortical Layer 5  
564 Neurons That Differ in Brain-wide Connectivity and Function. *Neuron* 88:1253–1267 Available  
565 at: <https://www.sciencedirect.com/science/article/pii/S0896627315009812> [Accessed  
566 September 4, 2018].

567 Kinoshita A, Tomimoto H, Tachibana N, Suenaga T, Kawamata T, Kimura T, Akiguchi I, Kimura J (1996)  
568 A case of primary progressive aphasia with abnormally ubiquitinated neurites in the cerebral  
569 cortex. *Acta Neuropathol* 92:520–524 Available at:  
570 <http://link.springer.com/10.1007/s004010050555> [Accessed January 15, 2019].

571 Knott GW, Quairiaux C, Genoud C, Welker E (2002) Formation of dendritic spines with GABAergic  
572 synapses induced by whisker stimulation in adult mice. *Neuron* 34:265–273 Available at:  
573 <http://www.ncbi.nlm.nih.gov/pubmed/11970868> [Accessed January 3, 2019].

574 Kramer MA, Roopun AK, Carracedo LM, Traub RD, Whittington MA, Kopell NJ (2008) Rhythm  
575 Generation through Period Concatenation in Rat Somatosensory Cortex Friston KJ, ed. *PLoS*  
576 *Comput Biol* 4:e1000169 Available at: <https://dx.plos.org/10.1371/journal.pcbi.1000169>  
577 [Accessed February 26, 2019].

578 Lee V, Maguire J (2014) The impact of tonic GABAA receptor-mediated inhibition on neuronal  
579 excitability varies across brain region and cell type. *Front Neural Circuits* 8:3 Available at:  
580 <http://journal.frontiersin.org/article/10.3389/fncir.2014.00003/abstract> [Accessed June 27,  
581 2018].

582 Magazzini L, Muthukumaraswamy SD, Campbell AE, Hamandi K, Lingford-Hughes A, Myers JFM, Nutt  
583 DJ, Sumner P, Wilson SJ, Singh KD (2016) Significant reductions in human visual gamma  
584 frequency by the gaba reuptake inhibitor tiagabine revealed by robust peak frequency  
585 estimation. *Hum Brain Mapp* 37:3882–3896 Available at:  
586 <http://www.ncbi.nlm.nih.gov/pubmed/27273695> [Accessed February 26, 2019].

587 Marreiros AC, Pinotsis DA, Brown P, Friston KJ (2015) DCM, Conductance Based Models and Clinical  
588 Applications. In, pp 43–70. Springer, Cham. Available at: [http://link.springer.com/10.1007/978-](http://link.springer.com/10.1007/978-3-319-20037-8_3)  
589 [3-319-20037-8\\_3](http://link.springer.com/10.1007/978-3-319-20037-8_3) [Accessed January 15, 2019].

590 Mathias S, Wetter TC, Steiger A, Lancel M (2001) The GABA uptake inhibitor tiagabine promotes slow  
591 wave sleep in normal elderly subjects. *Neurobiol Aging* 22:247–253 Available at:  
592 <http://www.ncbi.nlm.nih.gov/pubmed/11182474> [Accessed May 1, 2018].

593 Metherate R, Cruikshank SJ (1999) Thalamocortical inputs trigger a propagating envelope of gamma-  
594 band activity in auditory cortex in vitro. *Exp Brain Res* 126:160–174 Available at:  
595 <http://link.springer.com/10.1007/s002210050726> [Accessed June 19, 2018].

596 Michalareas G, Vezoli J, van Pelt S, Schoffelen J-M, Kennedy H, Fries P (2016) Alpha-Beta and Gamma  
597 Rhythms Subserve Feedback and Feedforward Influences among Human Visual Cortical Areas.  
598 *Neuron* 89:384–397 Available at: <http://www.ncbi.nlm.nih.gov/pubmed/26777277> [Accessed  
599 March 1, 2019].

600 Mody I, Pearce RA (2004) Diversity of inhibitory neurotransmission through GABAA receptors.  
601 *Trends Neurosci* 27:569–575 Available at:  
602 <https://www.sciencedirect.com/science/article/pii/S0166223604002279> [Accessed September  
603 11, 2018].

604 Mongillo G, Rumpel S, Loewenstein Y (2018) Inhibitory connectivity defines the realm of excitatory  
605 plasticity. *Nat Neurosci* 21:1463–1470 Available at: [http://www.nature.com/articles/s41593-](http://www.nature.com/articles/s41593-018-0226-x)  
606 [018-0226-x](http://www.nature.com/articles/s41593-018-0226-x) [Accessed December 5, 2018].

607 Moran R, Pinotsis DA, Friston K (2013) Neural masses and fields in dynamic causal modeling. *Front*  
608 *Comput Neurosci* 7:57 Available at:  
609 <http://journal.frontiersin.org/article/10.3389/fncom.2013.00057/abstract> [Accessed January 3,  
610 2019].

611 Moran RJ, Symmonds M, Dolan RJ, Friston KJ (2014) The Brain Ages Optimally to Model Its  
612 Environment: Evidence from Sensory Learning over the Adult Lifespan Sporns O, ed. *PLoS*  
613 *Comput Biol* 10:e1003422 Available at: <https://dx.plos.org/10.1371/journal.pcbi.1003422>  
614 [Accessed February 26, 2019].

615 Murley AG, Rowe JB (2018) Neurotransmitter deficits from frontotemporal lobar degeneration. *Brain*  
616 141:1263–1285 Available at: <https://academic.oup.com/brain/article/141/5/1263/4823510>  
617 [Accessed October 24, 2018].

618 Muthukumaraswamy SD, Myers JFM, Wilson SJ, Nutt DJ, Hamandi K, Lingford-Hughes A, Singh KD  
619 (2013a) Elevating Endogenous GABA Levels with GAT-1 Blockade Modulates Evoked but Not  
620 Induced Responses in Human Visual Cortex. *Neuropsychopharmacology* 38:1105–1112  
621 Available at: <http://www.nature.com/articles/npp20139> [Accessed May 1, 2018].

622 Muthukumaraswamy SD, Myers JFM, Wilson SJ, Nutt DJ, Lingford-Hughes A, Singh KD, Hamandi K  
623 (2013b) The effects of elevated endogenous GABA levels on movement-related network  
624 oscillations. *Neuroimage* 66:36–41 Available at:  
625 <https://www.sciencedirect.com/science/article/pii/S1053811912010579?via%3Dihub>  
626 [Accessed February 26, 2019].

627 Muthukumaraswamy SD, Shaw AD, Jackson LE, Hall J, Moran R, Saxena N (2015) Evidence that  
628 Subanesthetic Doses of Ketamine Cause Sustained Disruptions of NMDA and AMPA-Mediated  
629 Frontoparietal Connectivity in Humans. *J Neurosci* 35:11694–11706 Available at:  
630 <http://www.ncbi.nlm.nih.gov/pubmed/26290246> [Accessed January 14, 2019].

631 Naatanen R, Kujala T, Kreegipuu K, Carlson S, Escera C, Baldeweg T, Ponton C (2011) The mismatch

632 negativity: an index of cognitive decline in neuropsychiatric and neurological diseases and in  
633 ageing. *Brain* 134:3435–3453 Available at: [https://academic.oup.com/brain/article-](https://academic.oup.com/brain/article-lookup/doi/10.1093/brain/awr064)  
634 [lookup/doi/10.1093/brain/awr064](https://academic.oup.com/brain/article-lookup/doi/10.1093/brain/awr064) [Accessed February 26, 2019].

635 Nutt D, Wilson S, Lingford-Hughes A, Myers J, Papadopoulos A, Muthukumaraswamy S (2015)  
636 Differences between magnetoencephalographic (MEG) spectral profiles of drugs acting on  
637 GABA at synaptic and extrasynaptic sites: A study in healthy volunteers. *Neuropharmacology*  
638 88:155–163 Available at:  
639 <https://www.sciencedirect.com/science/article/pii/S0028390814003001> [Accessed January 3,  
640 2019].

641 Pascual-Marqui RD, Michel CM, Lehmann D (1994) Low resolution electromagnetic tomography: a  
642 new method for localizing electrical activity in the brain. *Int J Psychophysiol* 18:49–65 Available  
643 at: <http://linkinghub.elsevier.com/retrieve/pii/016787608490014X> [Accessed December 18,  
644 2018].

645 Phillips HN, Blenkmann A, Hughes LE, Bekinschtein TA, Rowe JB (2015) Hierarchical Organization of  
646 Frontotemporal Networks for the Prediction of Stimuli across Multiple Dimensions. *J Neurosci*  
647 35:9255–9264 Available at: <http://www.ncbi.nlm.nih.gov/pubmed/26109651> [Accessed May 1,  
648 2018].

649 Phillips HN, Blenkmann A, Hughes LE, Kochen S, Bekinschtein TA, Cam-CAN, Rowe JB (2016)  
650 Convergent evidence for hierarchical prediction networks from human electrocorticography  
651 and magnetoencephalography. *Cortex* 82:192–205 Available at:  
652 <https://www.sciencedirect.com/science/article/pii/S0010945216301058#fig3> [Accessed  
653 January 15, 2019].

654 Port RG, Gaetz W, Bloy L, Wang D-J, Blaskey L, Kuschner ES, Levy SE, Brodtkin ES, Roberts TPL (2017)  
655 Exploring the relationship between cortical GABA concentrations, auditory gamma-band  
656 responses and development in ASD: Evidence for an altered maturational trajectory in ASD.

657 Autism Res 10:593–607 Available at: <http://www.ncbi.nlm.nih.gov/pubmed/27696740>  
658 [Accessed February 26, 2019].

659 Razi A, Kahan J, Rees G, Friston KJ (2015) Construct validation of a DCM for resting state fMRI.  
660 Neuroimage 106:1–14 Available at:  
661 <https://www.sciencedirect.com/science/article/pii/S1053811914009446> [Accessed September  
662 13, 2018].

663 Roopun AK, Kramer MA, Carracedo LM, Kaiser M, Davies CH, Traub RD, Kopell NJ, Whittington MA  
664 (2008a) Period concatenation underlies interactions between gamma and beta rhythms in  
665 neocortex. Front Cell Neurosci 2:1 Available at:  
666 <http://journal.frontiersin.org/article/10.3389/neuro.03.001.2008/abstract> [Accessed January 3,  
667 2019].

668 Roopun AK, Kramer MA, Carracedo LM, Kaiser M, Davies CH, Traub RD, Kopell NJ, Whittington MA  
669 (2008b) Temporal interactions between cortical rhythms. Front Neurosci 2:145–154 Available  
670 at: <http://journal.frontiersin.org/article/10.3389/neuro.01.034.2008/abstract> [Accessed  
671 January 3, 2019].

672 Roopun AK, LeBeau FEN, Rammell J, Cunningham MO, Traub RD, Whittington MA (2010) Cholinergic  
673 neuromodulation controls directed temporal communication in neocortex in vitro. Front  
674 Neural Circuits 4:8 Available at:  
675 <http://journal.frontiersin.org/article/10.3389/fncir.2010.00008/abstract> [Accessed June 19,  
676 2018].

677 Roopun AK, Middleton SJ, Cunningham MO, LeBeau FEN, Bibbig A, Whittington MA, Traub RD (2006)  
678 A beta2-frequency (20-30 Hz) oscillation in nonsynaptic networks of somatosensory cortex.  
679 Proc Natl Acad Sci U S A 103:15646–15650 Available at:  
680 <http://www.ncbi.nlm.nih.gov/pubmed/17030821> [Accessed February 26, 2019].

681 Rowe JB, Hughes LE, Barker RA, Owen AM (2010) Dynamic causal modelling of effective connectivity



682 from fMRI: Are results reproducible and sensitive to Parkinson's disease and its treatment?  
683 Neuroimage 52:1015–1026 Available at:  
684 <https://www.sciencedirect.com/science/article/pii/S105381190901369X> [Accessed March 1,  
685 2019].

686 Semyanov A, Walker MC, Kullmann DM, Silver RA (2004) Tonicly active GABAA receptors:  
687 modulating gain and maintaining the tone. Trends Neurosci 27:262–269 Available at:  
688 <https://www.sciencedirect.com/science/article/pii/S0166223604000906?via%3Dihub>  
689 [Accessed June 18, 2018].

690 Shaw AD, Hughes LE, Moran RJ, Coyle-Gilchrist I, Rittman T, Rowe JB (2018) In vivo assay of cortical  
691 microcircuitry in frontotemporal dementia: a platform for experimental medicine studies.  
692 bioRxiv:416388 Available at: <https://www.biorxiv.org/content/early/2018/09/13/416388.short>  
693 [Accessed November 7, 2018].

694 Shaw AD, Moran RJ, Muthukumaraswamy SD, Brealy J, Linden DE, Friston KJ, Singh KD (2017)  
695 Neurophysiologically-informed markers of individual variability and pharmacological  
696 manipulation of human cortical gamma. Neuroimage 161:19–31 Available at:  
697 <http://www.ncbi.nlm.nih.gov/pubmed/28807873> [Accessed January 14, 2019].

698 Shipp S (2016) Neural Elements for Predictive Coding. Front Psychol 7:1792 Available at:  
699 <http://journal.frontiersin.org/article/10.3389/fpsyg.2016.01792/full> [Accessed January 14,  
700 2019].

701 Spriggs MJ, Sumner RL, McMillan RL, Moran RJ, Kirk IJ, Muthukumaraswamy SD (2018) Indexing  
702 sensory plasticity: Evidence for distinct Predictive Coding and Hebbian learning mechanisms in  
703 the cerebral cortex. Neuroimage 176:290–300 Available at:  
704 <https://www.sciencedirect.com/science/article/pii/S105381191830380X> [Accessed January 15,  
705 2019].

706 Stephan KE, Iglesias S, Heinzle J, Diaconescu AO (2015) Translational Perspectives for Computational

707 Neuroimaging. *Neuron* 87:716–732 Available at:  
708 <https://www.sciencedirect.com/science/article/pii/S0896627315006303> [Accessed February  
709 26, 2019].

710 Stephan KE, Kasper L, Harrison LM, Daunizeau J, den Ouden HEM, Breakspear M, Friston KJ (2008)  
711 Nonlinear dynamic causal models for fMRI. *Neuroimage* 42:649–662 Available at:  
712 <https://www.sciencedirect.com/science/article/pii/S1053811908005983> [Accessed February  
713 26, 2019].

714 Sukov W, Barth DS (2001) Cellular mechanisms of thalamically evoked gamma oscillations in auditory  
715 cortex. *J Neurophysiol* 85:1235–1245 Available at:  
716 <http://www.physiology.org/doi/10.1152/jn.2001.85.3.1235> [Accessed June 18, 2018].

717 Symmonds M, Moran CH, Leite MI, Buckley C, Irani SR, Stephan KE, Friston KJ, Moran RJ (2018) Ion  
718 channels in EEG: isolating channel dysfunction in NMDA receptor antibody encephalitis. *Brain*  
719 141:1691–1702 Available at: <https://academic.oup.com/brain/article/141/6/1691/4990439>  
720 [Accessed July 8, 2019].

721 Whittington M., Traub R., Kopell N, Ermentrout B, Buhl E. (2000) Inhibition-based rhythms:  
722 experimental and mathematical observations on network dynamics. *Int J Psychophysiol*  
723 38:315–336.

724 Whittington MA, Cunningham MO, LeBeau FEN, Racca C, Traub RD (2011) Multiple origins of the  
725 cortical gamma rhythm. *Dev Neurobiol* 71:92–106 Available at:  
726 <http://doi.wiley.com/10.1002/dneu.20814> [Accessed September 4, 2018].

727 Wu X, Huang L, Wu Z, Zhang C, Jiang D, Bai Y, Wang Y, Chen G (2013) Homeostatic competition  
728 between phasic and tonic inhibition. *J Biol Chem* 288:25053–25065 Available at:  
729 <http://www.ncbi.nlm.nih.gov/pubmed/23839941> [Accessed June 27, 2018].

730 Wyss C, Tse DHY, Komater M, Dammers J, Achermann R, Shah NJ, Kawohl W, Neuner I (2017) GABA

731 metabolism and its role in gamma-band oscillatory activity during auditory processing: An MRS  
732 and EEG study. *Hum Brain Mapp* 38:3975–3987 Available at:  
733 <http://www.ncbi.nlm.nih.gov/pubmed/28480987> [Accessed February 26, 2019].

734 Zeidman P, Jafarian A, Seghier ML, Litvak V, Cagnan H, Price CJ, Friston KJ (2019) A guide to group  
735 effective connectivity analysis, part 2: Second level analysis with PEB. *Neuroimage* 200:12–25  
736 Available at: <https://www.sciencedirect.com/science/article/pii/S1053811919305233>  
737 [Accessed October 9, 2019].

738

739

740 **Figure Legends**

741 *Figure 1. The neuronal model.*

742 a. Intrinsic connectivities found in all nodes between layer 4 stellates (ss), inhibitory interneurons (ii),  
743 superficial pyramidal modules (sp) and deep pyramidal modules (dp).

744 b. All 6 nodes used are represented as a network on the left, showing the extrinsic connectivities  
745 (solid line = forward; dotted line = backward; dashed line = lateral). A left hemisphere representation  
746 of these bilateral nodes in primary auditory cortex, superior temporal gyrus and inferior-frontal  
747 gyrus (light, medium and dark grey, respectively).

748 c. A detailed view of the extrinsic population connections for forward (solid lines) and backward  
749 (dotted lines) connections.

750 d. Matrices of the extrinsic and intrinsic connectivity weights, all of which had a permitted variance  
751 of 1/16.

752 e. A process flow describing the steps taken in the meta-analysis phase.

753

754 *Figure 2. Event Related Fields (ERFs).*

755 a. Mean ERFs across all subjects for all six nodes for the standard and deviant trials from 0-380ms.

756 The difference wave (MMN) is also shown. ERFs from the placebo condition are shown in blue and  
757 from the tiagabine condition in red. Significant changes with time across the drug condition are  
758 shown as a thick black line within each axis ( $p < 0.05$ , Bonferroni corrected for 6 regions). Shaded  
759 areas represent the standard error (SEM).

760 b. Significant differences for induced spectra power were found in the alpha ( $\alpha$ ), beta ( $\beta$ ) and lower  
761 and higher gamma bands ( $\gamma_1$  and  $\gamma_2$ ) (FWE cluster corrected at  $p < 0.001$ ). Here they are shown as flat  
762 scalp maps (lower plots) with rostro-caudal activity *versus* time (upper plots). The time axis runs  
763 from 0–380 ms post-stimulus.

764 c. Source-reconstructed T-contrasts ( $p < 0.001$ ) created for those frequency bands showing spatial  
765 changes across the drug condition in the 135 – 235 ms time window.

766

767 *Figure 3. Comparison between model and data.*

768 a. Residual differences between the observed and model-generated ERFs are shown for both the  
769 standard 4-cell conductance-based DCM and the ext-DCM. ERFs from all nodes for every subject are  
770 concatenated along the y-axis.

771 b. Bayesian model comparison of the 4-cell conductance-based DCM and the ext-DCM favours the  
772 ext-DCM, plotted here in terms of the posterior model probability (RFX Bayes Factor = 40.6).

773 c. Predicted ERFs are shown for the standard and deviant conditions, along with the difference wave  
774 (Std–Dev). The placebo and tiagabine conditions are depicted in blue and red respectively with  
775 significant differences ( $p < 0.05$ , Bonferroni corrected for 6 regions) shown as a thick black line within  
776 each axis.

777 d. Correlation coefficient between prediction and data for each node and each condition. Boxplots  
778 represent the distribution over subjects with small dots representing outliers and larger black circles  
779 representing the correlation coefficient of the meaned response of all subjects for each node and  
780 each condition.

781

782 *Figure 4. Prediction of hidden states.*

783 a. Significant differences in the modulation of GABA-A synaptic scaling for each of the three  
784 symmetric nodes. Green/red show significantly greater/lesser GABA-A synaptic scaling for tiagabine  
785 than the placebo. Posterior probability p-values are shown next to each connection.

786 b. To explore the functional differentiation between regions during the task conditions with respect  
787 to tonic inhibition, tonic GABA-A scaling on deep interneurons in IFG, STG and Aud, for each

788 individual is plotted for the placebo and tiagabine conditions. The standard and deviant conditions  
789 are plotted separately in the left and right columns respectively. Pair-wise Bayesian t-test statistics  
790 are reported on each plot, showing the Bayes Factor for each of the 6 comparisons. When there is  
791 evidence for a difference, or evidence for no difference, the Bayes factor is shown in green or blue  
792 respectively.

793 c. The correlation demonstrates the dynamic balance that persists between phasic and tonic  
794 inhibition (see main text discussion). Linear fit with 95% confidence bounds for tonic GABA-A scaling  
795 on deep inhibitory neurons vs phasic GABA-A scaling from deep inhibitory neurons to thalamic  
796 projecting pyramidal (Bayesian correlation pairs, Bayes factor=398.43).

797

798

799 *Table 1. Model parameters.*

800 Parameter values used by the neuronal model are shown with their permitted variances.

801

Parameter grouping	Parameter	Initial value	Permitted variance
Decay Constants, $\tau$ (ms)	AMPA $\tau$	4	1/16
	NMDA $\tau$	100	1/16
	GABAA $\tau$	16	1/8
	GABAB $\tau$	200	1/8
	$I_M \tau$	160	0
	$I_H \tau$	100	0
Misc. strengths	K <sup>+</sup> leak G	1	0
	Background V	2.17	1/32
Reversal potentials (mV)	Na <sup>2+</sup> reversal	60	0
	Ca <sup>2+</sup> reversal	10	0
	Cl <sup>-</sup> reversal	-90	0
	K <sup>+</sup> reversal	-70	0
	$I_H$ reversal	-100	0
Firing threshold (mV)	$V_T$ (all pops)	-40	0
Firing precision	$V_X$ (all pops)	1	1/32
$I_H$ I-V slope	$V_{HX}$	300	0
Cell Capacitances (pF)	$ss_C$	200	1/32
	$sp_C$	150	1/32
	$si_C$	50	1/32
	$dp_C$	400	1/32
	$di_C$	50	1/32
	$tp_C$	200	1/32
Delays (ms)	intrinsic	2	1/32
	extrinsic cortico-cortical	16	1/32
	extrinsic thalamo- cortical	80	1/32

Table 1

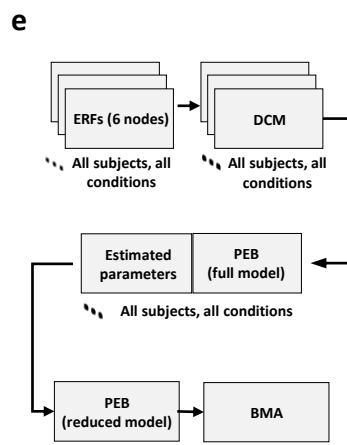
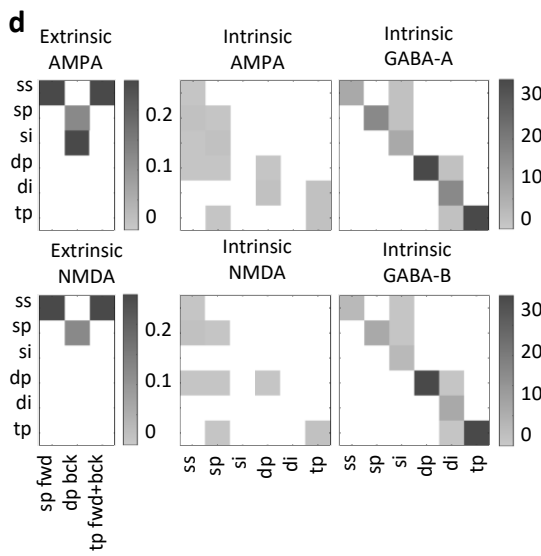
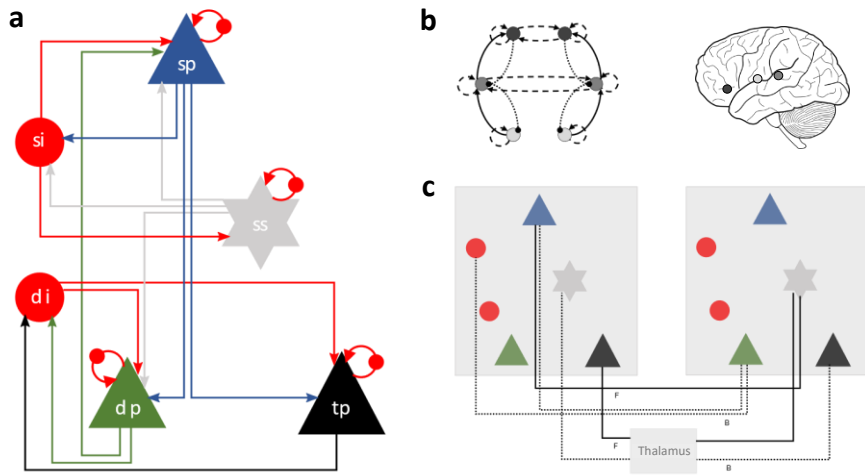
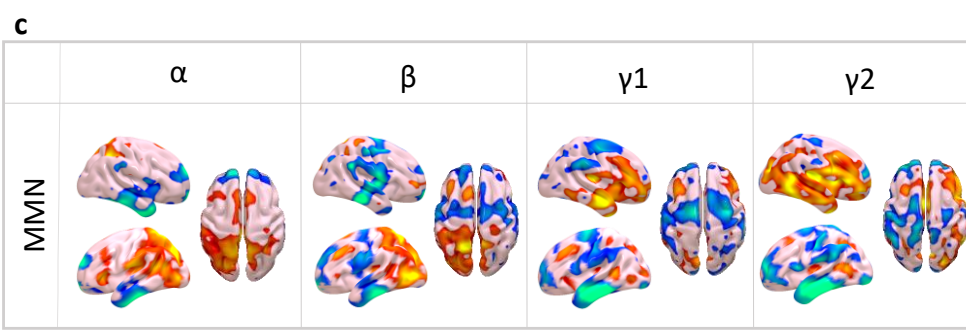
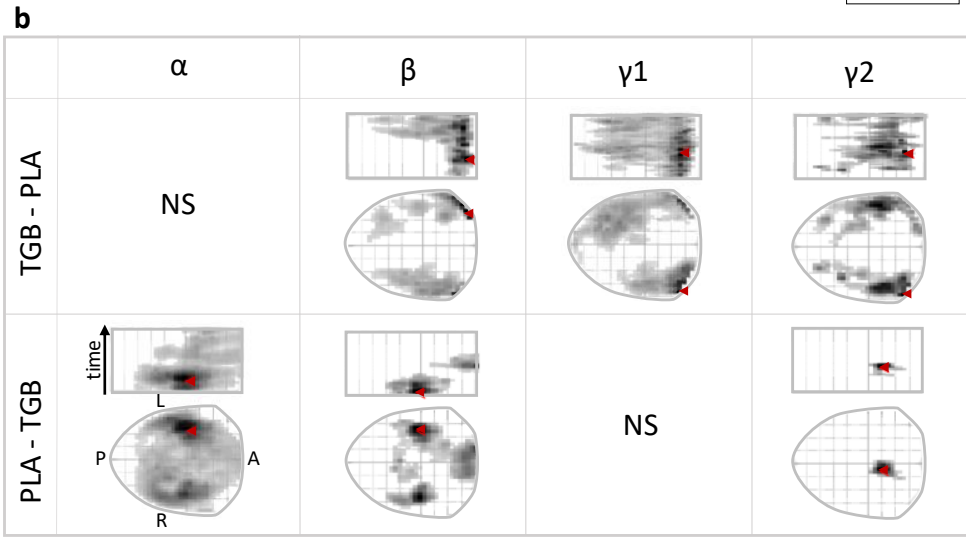
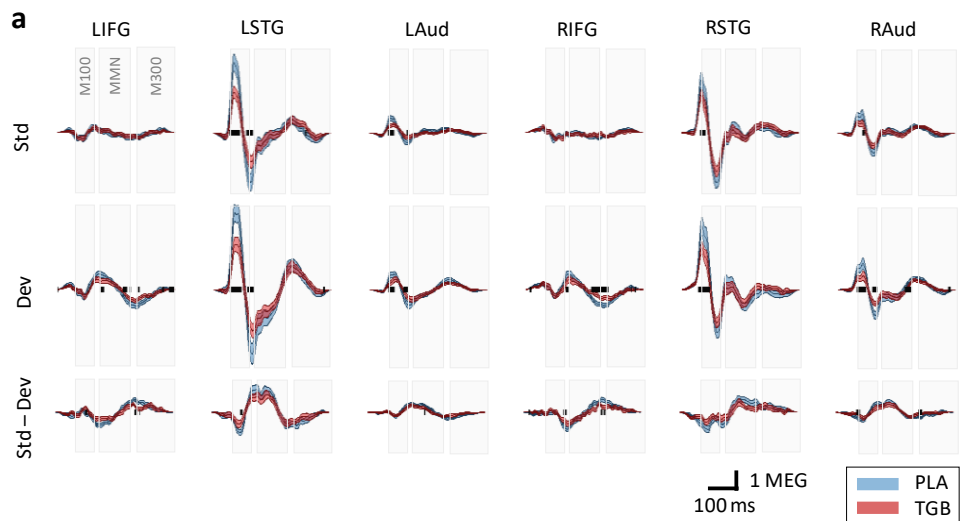


Figure 1





3.31      15

Figure 2

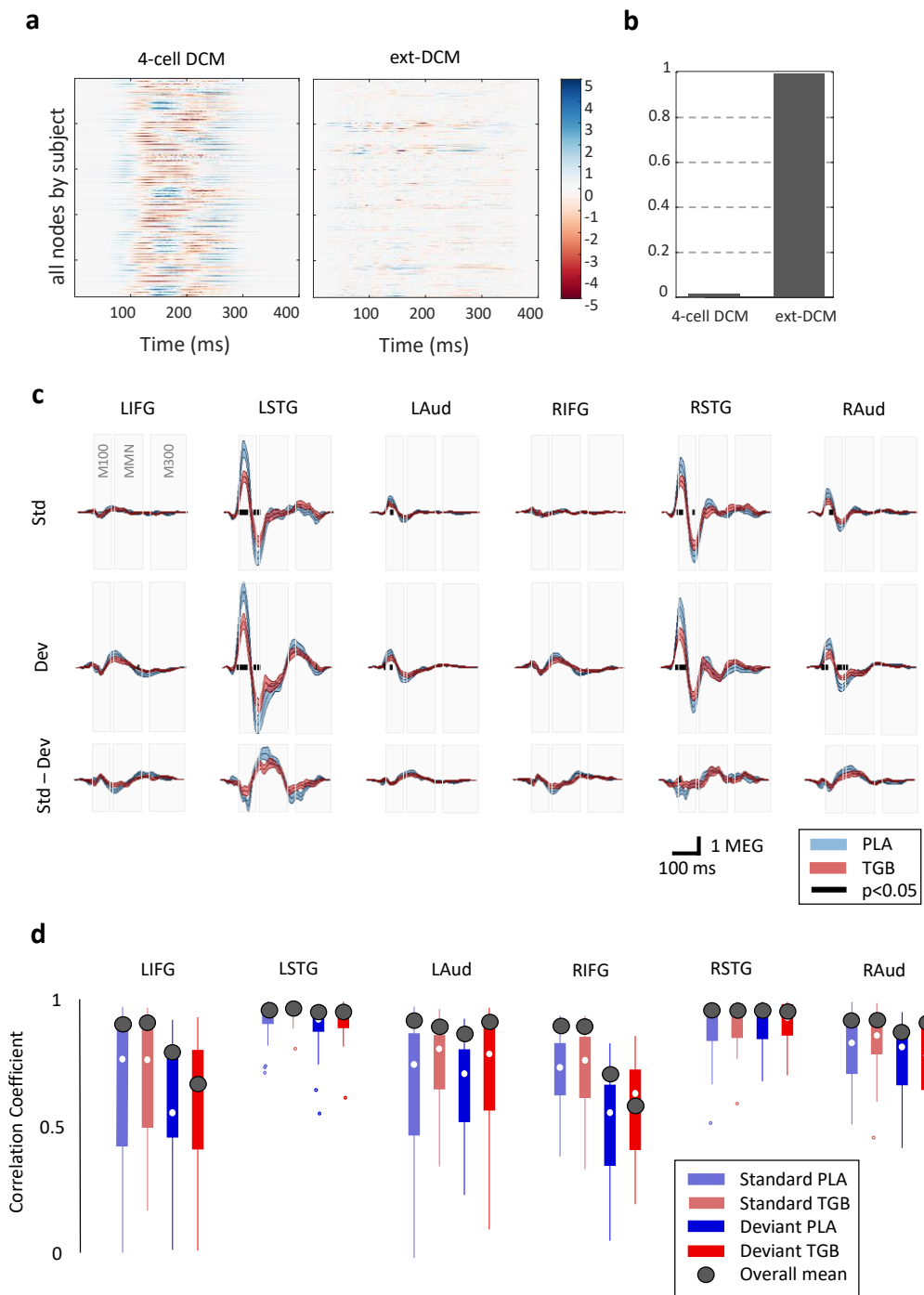


Figure 3

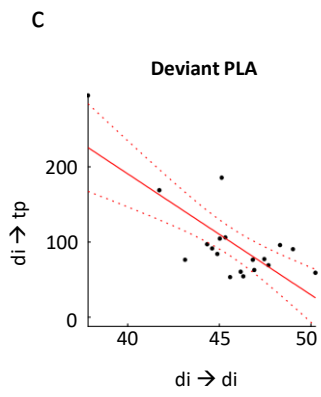
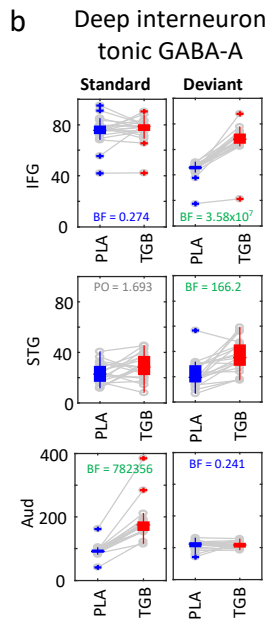
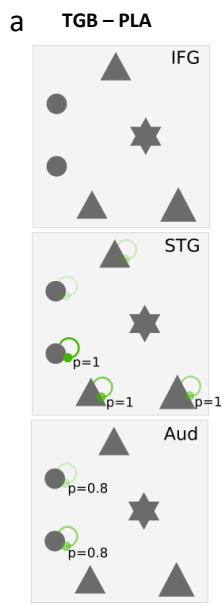


Figure 4